Geoscience Frontiers 6 (2015) 825–836

HOSTED BY

Contents lists available at ScienceDirect

China University of Geosciences (Beijing)

Geoscience Frontiers

journal homepage: www.elsevier.com/locate/gsf

Research paper

Preparation of earthquake-triggered landslide inventory maps using remote sensing and GIS technologies: Principles and case studies

Chong Xu*

Key Laboratory of Active Tectonics and Volcano, Institute of Geology, China Earthquake Administration, 1# Huayanli, Chaoyang District, PO Box 9803, Beijing 100029, China

ARTICLE INFO

Article history:
Received 8 August 2013
Received in revised form
9 January 2014
Accepted 11 March 2014
Available online 25 March 2014

Keywords:
Earthquake-triggered landslides
Inventory
Principle
GIS
Aerial photographs
Satellite images

ABSTRACT

Inventory maps of earthquake-triggered landslides can be constructed using several methods, which are often subject to obvious differences due to lack of commonly accepted criteria or principles. To solve this problem, the author describes the principles for preparing inventory maps of earthquake-triggered landslides, focusing on varied methods and their criteria. The principles include the following key points: all landslides should be mapped as long as they can be recognized from images; both the boundary and source area position of landslides should be mapped; spatial distribution pattern of earthquake-triggered landslides should be continuous; complex landslides should be divided into distinct groups; three types of errors such as precision of the location and boundary of landslides, false positive errors, and false negative errors of earthquake-triggered landslide inventories should be controlled and reduced; and inventories of co-seismic landslides should be constructed by the visual interpretation method rather than automatic extraction of satellite images or/and aerial photographs. In addition, selection of remote sensing images and creation of landslides attribute database are also discussed in this paper. Then the author applies these principles to produce inventory maps of four events: the 12 May 2008 Wenchuan, China M_w 7.9, 14 April 2010 Yushu, China M_w 6.9, 12 January 2010 Haiti M_w 7.0, and 2007 Aysén Fjord, Chile M_w 6.2. The results show obvious differences in comparison with previous studies by other researchers, which again attest to the necessity of establishment of unified principles for preparation of inventory maps of earthquake-triggered landslides.

1. Introduction

Preparation of inventory maps is an essential part of landslide hazard analysis (Harp et al., 2011a; Guzzetti et al., 2012), such as spatial distribution statistics of landslides (Xu and Xu, 2012a; Xu et al., 2014c), susceptibility (Pradhan and Lee, 2010; Pourghasemi et al., 2012; Xu, 2013a), hazard assessment (Pradhan and Lee, 2007; Xu et al., 2012a, b), and river and landform evolution in earthquake-struck areas with widespread and intensive landslides (Parker et al., 2011; Xu and Xu, 2013). A landslide inventory map portrays the location, numbers and other data of occurrence and the types of mass movements that have left discernable traces in an area (Guzzetti et al., 2012). Such maps can be prepared by using various techniques. Qualities (e.g. completeness and validity) of these inventory maps determine the objectivity and accuracy of subsequent research results. Earthquakes often trigger a large number of landslides (Keefer, 1984; Rodriguez et al., 1999; Mahesh et al., 2011; Martha et al., 2015) and a number of inventory maps of landslides triggered by earthquakes have been prepared (e.g. Khazai and Sitar, 2004; Xu et al., 2010, 2014c). It should be noted that there were often obvious differences in landslide inventory maps prepared by different researchers for the same seismic event. In addition to differences of the methods used, one possible reason for this problem is a lack of criteria for the preparation and update of earthquake-triggered landslide inventory maps.

In the current paper, the author describes the principles for preparing inventory maps of earthquake-triggered landslides, focusing on varied methods and their criteria. In the following text, the author uses the terms “inventory” and “inventory map” with the same meaning (e.g. Guzzetti et al., 2012). The principles

* Tel./fax: +86 10 62009084.
E-mail addresses: xc11111111@126.com, xuchong@ies.ac.cn.
Peer-review under responsibility of China University of Geosciences (Beijing)

1674-9871/$ – see front matter © 2015, China University of Geosciences (Beijing) and Peking University. Production and hosting by Elsevier B.V. All rights reserved.
http://dx.doi.org/10.1016/j.gsf.2014.03.004

include the following criteria: all landslides should be mapped as long as they can be recognized from images; both the boundary and source area position of landslides should be mapped; spatial distribution pattern of earthquake-triggered landslides should be continuous; complex landslides should be divided into distinct groups; three types of errors such as precision of the location and boundary of landslides, false positive errors, and false negative errors of earthquake-triggered landslide inventories should be controlled and reduced; and inventories of co-seismic landslides should be constructed by the visual interpretation method rather than automatic extraction of satellite images. In addition, selecting remote sensing images and building landslides attribute database are also discussed in this paper. Then these principles were applied to prepare inventory maps for four events in the beginning of the 21st century: the 12 May 2008 Wenchuan, China M_w 7.9, 14 April 2010 Yushu, China M_w 6.9, 12 January 2010 Haiti M_w 7.0, and 2007 Aysén Fjord, Chile M_w 6.2. The results show obvious differences in comparison with previous studies by other researchers, which again attest to the necessity of establishment of unified principles for preparation of earthquake-triggered landslide inventory maps.

2. Overview of principles for preparing earthquake-triggered landslide inventory maps

2.1. Methods

An earthquake-triggered landslide inventory map can be prepared by several methods, including field investigations, visual interpretation of aerial photographs, digitizing paper-based landslide inventories, computer screen-based visual interpretation of high-resolution remote sensing images, and automatic extraction from remote sensing images.

2.1.1. Field investigations

This method was widely used before the remote sensing technology emerged. Based on observations in the field, researchers delineate or locate earthquake-triggered landslides on topographic maps, geologic maps, or other thematic maps, and thus prepare associated earthquake-triggered landslide distribution maps. For example, the 1783 Calabria, Italy M 7.0 earthquake is considered to be the first case study with the earthquake-triggered landslide inventory map based on field investigations in the epicenter area (Keefer, 2002). Three limitations of this method should be noted: (1) Landslide inventories based on field investigations often aim at landslides of large or moderate sizes, while those of small sizes are often ignored, resulting in rough and incomplete landslide inventories (Guzzetti et al., 2012). (2) Earthquake-triggered landslides are generally widespread distributed and of high densely in broad earthquake stuck areas, which often result in powerless to prepare detailed landslide inventories only based on filed investigations. (3) The resulting landslide distribution maps with topographic and geologic background (earthquake-triggered landslides are drawn on paper-based thematic maps) can not directly be used in subsequent calculation of the landslide number and area, landslide spatial distribution analysis, and hazard assessments. However, recently, the filed investigation methods were also used in preparing landslide inventory maps related to moderate earthquakes (Alfaro et al., 2012; Jibson and Harp, 2012), or only as a verification tool for a small part of landslides triggered by large earthquakes (Harp et al., 2011b; Xu et al., 2014c). Anyway, it is almost impossible only rely on field investigations to prepare complete and detailed inventories of earthquake-triggered landslides.

2.1.2. Visual interpretation of aerial photographs

With the advent of the remote sensing technology, visual interpretation of remote sensing images, saving a large amount of field work, has become the main method for preparation of landslide inventories. Early remote sensing images are mainly aerial photographs. Using this method, positions or boundaries of landslides are directly plotted on aerial photographs or other thematic maps based on visual interpretation. Landslide inventories based on this method can avoid missing a large number of landslides on small scales and can obtain detailed and comprehensive earthquake-triggered landslide inventories. These landslide inventories are, however, also paper-based materials rather than compute-based digital files of vector format. Therefore, the inventories also can not directly be used for subsequent spatial analysis because it is difficult to obtain precise numbers and areas of landslides in the case that a large number of landslides are triggered by a major earthquake. This method was applied in the analyses of several earthquake events (Keefer, 2002), such as the 1948 M 7.3 Fukui, Japan earthquake, the May 31, 1970 M 7.9 Rio Santa earthquake of Peru, and the February 4, 1976 M 7.5 Guatemala earthquake. It should be noted that field investigations are often an auxiliary tool for visual interpretation of aerial photographs associated with earthquake-triggered landslides.

2.1.3. Digitizing of paper-based landslide inventories

This technique is an advanced stage of paper-based earthquake-triggered landslide inventories. With the development of the computer and geographic information system (GIS) technologies, paper-based landslide inventories can be digitalized for subsequent earthquake-triggered landslide studies, such as spatial distribution analysis, landslides hazard assessment, and evolution of rivers and landforms in areas affected by widespread co-seismic landslides. The resulting digital inventory maps have a high degree of usefulness and play an important role in promoting studies of earthquake-triggered landslides. The first well-known digital inventory map for earthquake-triggered landslides was compiled by Harp and Jibson (1995, 1996), in which large amount of landslides triggered by the 17 January 1994 M_w 6.7 Northridge earthquake were mapped from visual interpretation of aerial photography and selected field verification. Their results of digitalizing landslide inventories showed more than 11,000 landslides triggered by the Northridge earthquake.

2.1.4. Computer screen-based visual interpretation of high-resolution remote sensing images

Computer screen-based visual interpretation of high-resolution remote sensing images (especially high-resolution satellite images) is the most popular method for preparing earthquake-triggered landslide inventory maps currently. With the computer and GIS technologies becoming highly matured and steady development of remote sensing technology, a plenty of commercial satellites come into service and masses of high-resolution satellite images are available. They have greatly improved the methods of preparing earthquake-triggered landslide inventory maps. The conditions based on paper-based remote sensing images are changed into syntheses of computer screen-based landslide visual interpretation based on GIS software and digital satellite images and aerial photographs, and construction of vector landslides inventory maps. In this method, at first, remote sensing images are precisely geographically registered; then landslides can be mapped based on the registered satellite images on a GIS platform. In addition, landslide inventory maps can be prepared based on three-dimensional perspective of the digital elevation model (DEM) for more precise and objective visual interpretation. Recently, this method has become the most popular tool for earthquake-

triggered landslide inventory mapping (Xu et al., 2009a, b, 2014c; Dai et al., 2011; Gorum et al., 2011). The resulting digital landslide inventory maps can be directly used for subsequent analysis of spatial distribution and hazard assessment of landslides triggered by earthquakes.

2.1.5. Automatic extraction from remote sensing images

Based on advanced remote sensing image processing technologies, objects including landslides, water, residential areas, and forests can be separated by data processing and mathematic analysis. There are several advantages of this method such as high efficiency and adjustable thresholds, and several attempts (Martha et al., 2012; Moosavi et al., 2014) showed quite high accuracy. However, there were obvious errors appearing in results by using earthquake-triggered landslides automatic extraction related to the 2008 Wenchuan earthquake (Parker et al., 2011; Xu et al., 2014c). Pre-earthquake landslides, bare rocks, roads, and resident districts are easily extracted and mixed into co-seismic landslides. The resultant automatic extraction-based landslide inventories may be difficult to be applied to subsequent earthquake-triggered landslide hazard analysis. Currently, this issue has received much attention of researchers, and perhaps significant improvements to this problem would be generated in the near future.

Although the visual interpretation method seems dominant in preparation of earthquake-triggered landslide inventory maps, field investigations can not be ignored. Because some objects, including landslides, recognized from aerial photographs or remote sensing images should be verified by inspection in the field to prove their objectivity.

2.2. Earthquake-triggered landslide inventory maps

During recent decades, many earthquake-triggered landslide inventory maps have been constructed for landslide hazard assessment. The typical examples include the 2008 Wenchuan, China earthquake, 2004 Niigata, Japan earthquake, and the 2010 Haiti earthquake. Table 1 shows a list of landslide inventories related to 25 earthquakes, which provided essential data for landslide spatial distribution analysis, landslide hazard assessment, and research of geomorphologic evolution in earthquake-struck areas. However, they are not comparable with each other, because these landslide inventories were compiled by different researchers under the condition without unified principles, thus having obvious differences in varied aspects.

3. Principles of preparing detailed landslide inventory maps

3.1. Landslide identification

(1) All landslides should be mapped as long as they can be recognized from images. Harp et al. (2011a) suggested an ideal landslide inventory should contain all of the landslides that are possible to detect down to sizes of 1–5 m in length. This is coincident with resolutions of current available satellite images. For example, the QuickBird image has a resolution of 0.46 m, ideally, when the landslide length large than 1–2 grids, the landslide can be recognized. Therefore, Harp et al. (2011a) considered the smallest scale of landslides is 1–5 m in length. In practice, we should not be restricted or affected by the smallest landslide scale threshold. The scale threshold depends on resolution of remote sensing images. For example, if moderate-resolution remote sensing images are used, such as ALOS (10 m resolution of multispectral images) and ASTER (15 m resolution of multispectral images), only landslides of length at least larger than 10–15 m can be detected. However, if images used have a resolution better than QuickBird, we can detect landslides in length of less than 1 m. An example is that the aerial photographs used for the inventory of landslides triggered by the 2010 Yushu, China earthquake have a resolution of 0.2 or 0.4 m (Xu et al., 2013a), allowing us to detect even smaller landslides less than 1 m in length. In some actual inventories, landslides of small scales, for example less than 10 m in length, often occupy a relatively small proportion. For instance, among multi-source remote sensing images used for landslide inventory mapping for the 2008 Wenchuan earthquake, there are several kinds of satellite images of 10 m resolution. However, the number of landslides areas larger than 400 m^2 (about four 10 m $\times$ 10 m grid) is rather small, which indicates the resulting inventory is robust and little affected by resolution of the remote sensing images used. Therefore, we should consider all landslides as long as they can be recognized on remote sensing images. In subsequent analysis, it is suggested that the area less than about four grids can be excluded from the inventory. Actually, these small landslides have little effects on subsequent research since the number and scale of these landslides are rather small.

(2) Both landslide boundaries and positions of landslide source area should be delineated and located. Before the GIS technology emerged, landslides were depicted by points or other symbols. For example, landslides triggered by the May 31, 1970 Peru earthquake (Plafker et al., 1971) and the 1989 Loma Prieta earthquake (Keefer, 2000) have been mapped with such symbols. The point inventories provide intuitive knowledge about spatial distribution of landslides, but no information about the landslide area and volume, which are useful for landslide spatial distribution statistics and subsequent research on river and geomorphologic evolution in earthquake-struck areas. Therefore, earthquake-triggered landslides should be mapped as polygons depicting their true shapes. In addition, to achieve better identification, the landslides source areas should be extracted and expressed as points or polygons. At present, delineating landslide source areas from remote sensing images is often subjective because the lower boundary of a source area of a landslide is difficult to recognize.

(3) Spatial distribution of landslides should be continuous. This includes two meanings: one is that there should be no image-covered blank areas, which is accepted by the majority of researchers. The other is that a few abnormal landslides scattered far away from the earthquake source should be excluded from the landslide inventory, because these landslides often occur on slopes which are highly prone to slide but with little relevance to the earthquake. In most cases, landslide spatial distribution shows a continuous feature as the earthquake is a central epicenter point or a fault line event. Earthquake shaking intensity has a decrease tendency outward from the epicenter. Therefore, the distribution of co-seismic landslides would have a roughly similar tendency to ground shaking intensity. Some researchers presented a loose relationship between peak ground acceleration (PGA) and seismic landslide occurrence. The continuity of a co-seismic landslide inventory map can help determine the minimum PGA values and the boundary of earthquake-triggered landslides. For example, for the 23 August 2011 Mineral, Virginia, M_w 5.8 earthquake, Jibson and Harp (2012) considered there are extraordinary distance limits of landslides triggered by the earthquake. Some single rocks and landslides of quite small sizes were mapped to prove the subject, which resulted in an extremely large landslide-limit-area. Therefore, the author suggests that the abnormal phenomenon related to the widespread spatial distribution of landslides triggered by the Virginia earthquake is mainly due to that the continuity of the landslide inventory was ignored. Recognizing the continuity of seismic landslide distribution allows one to delineate the real landslide distribution area objectively.

Table 1
Summary of earthquake-triggered landslide inventories.

No.	Country	Region	Date	M_w	M_s	Type	Number	Area (km^2)	References
1	China	Lushan	2013/4/20	6.6	7.0	Point	3878		Xu, 2013b
						Point	15,639		Xu and Xu, 2014a
2	Spain	Lorca	2011/5/11	5.1		Point	>250		Alfaro et al., 2012
3	China	Yushu	2010/4/14	6.9	7.1	Polygon	2036	1.194	Xu et al., 2013b; Xu and Xu, 2014b
						Point	282		Yin et al., 2010
4	Haiti	Port-au-prince	2010/1/12	7.0		Polygon	30,828	15.736	Xu and Xu, 2012b; Xu et al., 2012c, 2014a
						Point	>7000		Harp et al., 2011b
						Polygon	4490	8	Gorum et al., 2013
5	Japan	Iwate–Miyagi	2008/6/14	6.9	7.2	Point	4161	10.2	Yagi et al., 2009
6	China	Wenchuan County	2008/5/12	7.9	8.0	Polygon, Top point, Centroid	197,481	1160	Xu and Xu, 2012a; Xu et al., 2014c
						Polygon	56,000	811	Dai et al., 2011
						Polygon	48,007	711.8	Xu et al., 2009a, b
						Polygon	73,367	565.8	Parker et al., 2011
						Point	60,000		Gorum et al., 2011
						Point	<10,000		Qi et al., 2010
						Point	16,704		Huang and Li, 2009a
						Point	<10,000		Huang and Li, 2009b
7	Chile	Aysén Fjord	2007/1/22	6.2	6.3	Polygon	538	17	Sepúlveda et al., 2010
8	India–Pakistan	Kashmir	2005/10/8	7.6	7.7	Polygon	1293		Owen et al., 2008
						Point	2424		Sato et al., 2007
						Polygon	2252	61	Kamp et al., 2008
9	Japan	Niigata	2004/10/23	6.6	6.8	Polygon	1212	7.99	Wang et al., 2007
						Polygon	>1000		Chigira and Yagi, 2006
						Polygon	362		Sassa, 2005
						Polygon	1353		Sato et al., 2005
						Polygon	4438		Sekiguchi and Sato, 2006
10	China	Taiwan	1999/9/21	7.6	7.3	Polygon	~10,000		Liao and Lee, 2000; Wang et al., 2003; Khazai and Sitar, 2004
						Polygon	~20,000		Wang et al., 2002
11	Italy	Umbria–Marche	1997/9/26	6	5.9	Polygon	200		Marzorati et al., 2002
12	Japan	Hyogo-ken Nanbu	1995/1/17	6.9	6.8	Point	674		Fukuoka et al., 1997
13	America	Northridge, California	1994/1/17	6.7	6.8	Polygon	>11,000	23.8	Jibson and Harp, 1994; Harp and Jibson, 1996
14	America	Loma Prieta, California	1989/10/17	6.9	7.1	Point	>1046		Keefer, 2000
15	Ecuador		1987/3/5	7	6.9	Point			Tibaldi et al., 1995; Schuster et al., 1996
16	America	Coalinga	1983/5/2	6.2	6.7	Polygon			Harp et al., 2011a
17	Italy	Irpinia	1980/11/23	6.9	6.9	Polygon			Harp and Keefer, 1989; Wasowski et al., 2002
18	America	Mammoth Lakes, California	1980/05/25–27		6.1	Polygon	5200	6	Harp et al., 1984, 2011a
19	Italy	Friuli	1976/5/6		6.4	Point			Govi, 1977; Harp et al., 2011a
20	Guatemalan		1976/2/4		7.5	Polygon	50,000		Harp et al., 1978, 1981, 2011a
21	America	San Fernando, California	1971/2/9		6.5	Polygon	>1000		Morton, 1971; Harp et al., 2011a
22	Peru		1970/5/31	7.8	7.9	Point	>1000		Plafker et al., 1971; Harp et al., 2011a
23	Japan	Imaichi	1949/12/26		6.4	Point			Morimoto, 1951; Harp et al., 2011a
24	New Zealand	Murchison	1929/6/17	7.7	7.8	Point	>7400	200	Adams, 1980; Pearce and O'Loughlin, 1985; Pearce and Watson, 1986
25	America	New Madrid	1811/12/16	8.3	8.8	Point	>220		Jibson and Keefer, 1989

(4) Complex landslides should be divided into individual ones. Several landslides often occur on a natural slope because high density and large number of earthquake-triggered landslides. Coalescing landslides, showing two landslides or more joint together, was often be falsely delineated as an individual and complex landslide (e.g. Parise and Jibson, 2000; Parker et al., 2011). Although limitation of such operation will not lead to a change of the total area affected by landslides, obvious differences in landslide number and landslide volume will appear with respect to the actual situation, which can lead to large errors in the subsequent volume calculation of landslides. For example, the landslide volume related to the 2008 Wenchuan earthquake calculated by Parker et al. (2011) is larger than the actual situation because several individual landslides were mapped into one complex landslide in their inventory map. This issue is often ignored as previous studies do not consider the subsequent volume calculation of regional landslides. Therefore, it is important to map individual landslides rather than complex landslides for volume calculation. It needs to consider remote sensing image and topographic characteristics of landslides to distinguish individual landslides from a complex landslide. An individual landslide shows source area integrity consistency on the remote sensing image, and topography of the landslide shows performance of the same natural slope. Some landslides, which have the common source area and the same moving direction, have been delineated as an individual landslide even if movement paths are separated. If source areas of two landslides or more are separated, we should separate these landslides based on expert knowledge, remote sensing image and topographic characteristics, and selected field investigation even their accumulated materials are connected together. In short, the baseline of differentiation of individual landslides is to consider consistency of landslide material and integrity of landslides.

By considering this baseline, the error from using of "area-volume" power law formula to calculate landslide volume on a regional scale can be controlled. Several individual landslides in low-resolution images may be misjudged into a single larger landslide because the distances of them are less than the resolution of the image. Therefore, the higher resolution of the images used, the easier individual landslides are separated and the more objective landslide inventory maps prepared.

(5) Errors of landslide inventory should be controlled. Precision is an essential factor of landslide inventory quality. There are three aspects affecting the precision of landslide inventories: precision of the location and boundary of landslides, false positive errors (landslide errors, commission), and false negative errors (non-landslide errors, omission). Precision of the geographic location and boundary of landslides is related to qualities of base remote sensing images and carefulness of interpreters. Remote sensing images used to interpret landslides need to be subject to a series of manipulations including system calibration, ortho-rectification, and geometric precision correction. In principle, the error can not be greater than one grid size of the image. False positive errors mean non-landslides areas are considered to be landslides areas. These errors include recognizing pre-earthquake landslides, landslides occurring after the earthquake which may be caused by rainfall, artificial excavation, bare slopes, and terrace as co-seismic landslides. In order to reduce these errors, the time of pre- and post-earthquake remote sensing images collected for landslide interpretation should be close to the earthquake occurrence time so as to avoid pre-earthquake landslides and post-earthquake landslides triggered by rainfall or other triggers being mixed into co-seismic landslides. Artificial excavation, bare slopes, and terrace can be excluded by comparing landslide inventories with pre-earthquake remote sensing images. False negative errors mean co-seismic landslides are missed, which makes landslide inventories be incomplete. The reasons of false negative errors are that remote sensing images for landslide interpretation do not cover the whole earthquake-struck area, small landslides are not recognized, and coherent landslides such as deep-seated landslides are easily missed as they have no significant differences with the environments on images and limitation of experiments of landslide interpreters. Coherent landslides are difficult to distinguish from surroundings on images because vegetation still exists and only suffers relatively minor damage after occurrence of landslides.

It needs to further illustrate how to distinguish co-seismic landslides from pre-earthquake landslides and post-earthquake landslides triggered by rainfall or other triggers based on remote sensing images taken at pre- and post-earthquake times. If a landslide does not exist on the pre-earthquake image but exists on the image taken after the earthquake occurs, the landslide is considered to be a co-seismic landslide. If there are two remote sensing images taken after the earthquake at different times, a landslide exists on the image for long time after the earthquake but is absent on the image for short time after the earthquake, this landslide is considered to be a post-earthquake landslide which may be triggered by rainfall or other factors after the earthquake. If a landslide exists on both images taken before and after the earthquake and shows same morphology and texture, the landslide is not considered to be triggered by the earthquake. If they only show same morphology but different texture and color tones, we should consider more. If texture of the landslide on the two images shows obvious differences, especially the landslide shows more obvious differences from surroundings on the post-earthquake image, it is considered to be a co-seismic landslide. In turn, if a landslide shows more obvious differences from surroundings on pre-earthquake image than on the post-earthquake image, it is considered to be a pre-earthquake landslide because vegetation is recovering in the landslide area. If a landslide shows different morphology on images taken before and after the earthquake, it can be divided into two kinds of situations: if the area of a landslide on the post-earthquake image is larger than on the pre-earthquake image, it indicates the landslide enlargement and shows that it is a new landslide triggered by the earthquake. In contrary, if the area of the landslide on post-earthquake image is smaller than that on the pre-earthquake image, we should use color tone and texture to judge whether the landslides is triggered by the earthquake or not. If color tone of the landslide shows gradual change from its boundary to the center, the landslide is not considered to be triggered by the earthquake since vegetation is recovering. If the landslide of a smaller area on the post-earthquake image shows obvious differences, it should be a new co-seismic landslide occurring in the area of a previously existing landslide. Based on above analysis, we can objectively and accurately distinguish co-seismic landslides, pre-earthquake landslides, and post-earthquake landslides.

(6) In order to obtain detailed and complete earthquake-triggered landslide inventory maps, the visual interpretation method rather than automatic identification should be employed. Up to now, accuracy and robustness of results of earthquake-triggered landslide automatic extraction (e.g. Parker et al., 2011) are still relatively low and can not meet the requirement of subsequent hazard assessment and studies on river and geomorphic evolution in earthquake areas. This is due to the spectral characteristics of earthquake-triggered landslides are similar to other objects, such as exposed rocks, roads, and human settlements. Therefore, there are always errors in results from seismic landslide automatic extraction compared to that from visual interpretation. In my opinion, in the future, the visual interpretation method will be a more preferable method than the automatic information extraction method.

3.2. Selecting remote sensing images

It is essential to state the principles of remote sensing images selection for preparing landslide inventories. Harp et al. (2011a) have suggested some general principles for selecting remote sensing images. In addition, two more important points should be supplemented: First, images taken before the earthquake should be collected as soon as possible because the landslides occurred before the earthquake and false negative errors can be easily excluded from pre-earthquake remote sensing images. Second, Harp et al. (2011a) considered that the digital elevation model (DEM) is necessary; yet in my opinion, the DEM is less important for skilled landslide interpretation because landslides can be determined based on ridges and drainages on remote sensing images. Of course, DEM data for constructing three-dimensional view of post-earthquake landslides can be more convenient for primary interpreters. Three-dimensional scenes are important for interpretation of ancient deep-seated landslides. For recent co-seismic landslides, analysis of image texture and tone differences of landslides from surroundings is more effective for visual interpretation of co-seismic landslides than three-dimensional scenes. Here the author emphasizes how to select remote sensing images for landslide interpretation: (1) Images must be continuous and cover the entire area of the earthquake-struck area. (2) Resolution of images should be high enough to meet the requirements of small landslides interpretation. (3) Remote sensing images taken before an earthquake should be collected as much as possible. (4) Remote sensing images of pre-earthquake and post-earthquake should be obtained close to the time of earthquake occurrence for obtaining initial state of the terrain and infrastructure affected by the earthquake. In addition, images for landslide interpretation should not be covered by clouds.

3.3. Building landslides attribute database

A landslide inventory should contain attribute database, including landslide geometric attributes such as length, width, and height, slope angle, slope aspect, lithology, and classifications. Most principles of earthquake-triggered landslide classification (e.g. Keefer, 1984, 1999) are based on landslide classification by Varnes (1978). With regard to recent individual earthquake events, landslide classification is always simplified. Therefore, there are no unified principles for earthquake-triggered landslides classification. In addition, many co-seismic landslides show characteristics of two types of landslides or more and are difficult to be classified. Therefore, only parts of publications considered earthquake-triggered landslide classifications.

4. Case studies

Based on the aforementioned principles of landslides identification from remote sensing images, selecting remote sensing images, and building landslides attribute database, earthquake-triggered landslide inventories related to four recent major earthquakes were prepared. They are the 12 May 2008 Wenchuan, China M_w 7.9, 14 April 2010 Yushu, China M_w 6.9, 12 January 2010 Haiti M_w 7.0, and 21 April 2007 Aysén Fjord, Chile M_w 6.2.

4.1. The 12 May 2008 Wenchuan M_w 7.9 earthquake

This event occurred on the eastern margin of the Tibetan Plateau, abutting the Sichuan Basin in east. It produced three surface ruptures, among which the largest one is 240 km-long (Xu et al., 2009c; Tan et al., 2012). The earthquake triggered hundreds and thousands of landslides when the quake shook a broad mountain area with steep canyon terrain. Based on visual interpretation of high-resolutions satellite images and aerial photographs, and assisted by field investigations, I delineated 197,481 landslides in an area of 110,000 km^2, beginning several weeks after the earthquake and ended in 2012, over 4 years. These landslides cover a total area of 1160 km^2 (Fig. 1) and resulted in about 6.123×10^9 m^3 accumulation materials (Xu, 2013c). Multi-remote sensing images, used for the landslide inventory mapping, include aerial photos and satellite images in 1–5 m resolutions in most of the earthquake struck area (Xu et al., 2014c). Most of the landslides concentrated in an ellipse of 44,000 km^2 (Xu and Xu, 2012a; Xu et al., 2014c). In addition, centroids and top points of each landslide were extracted and located for constructing another two types of landslide inventories. Red patches in Fig. 1 present landslides triggered by the Wenchuan earthquake. Most of the landslides were distributed on the hanging wall of the seismogenic fault. It seems that the landslides on the southwestern section of

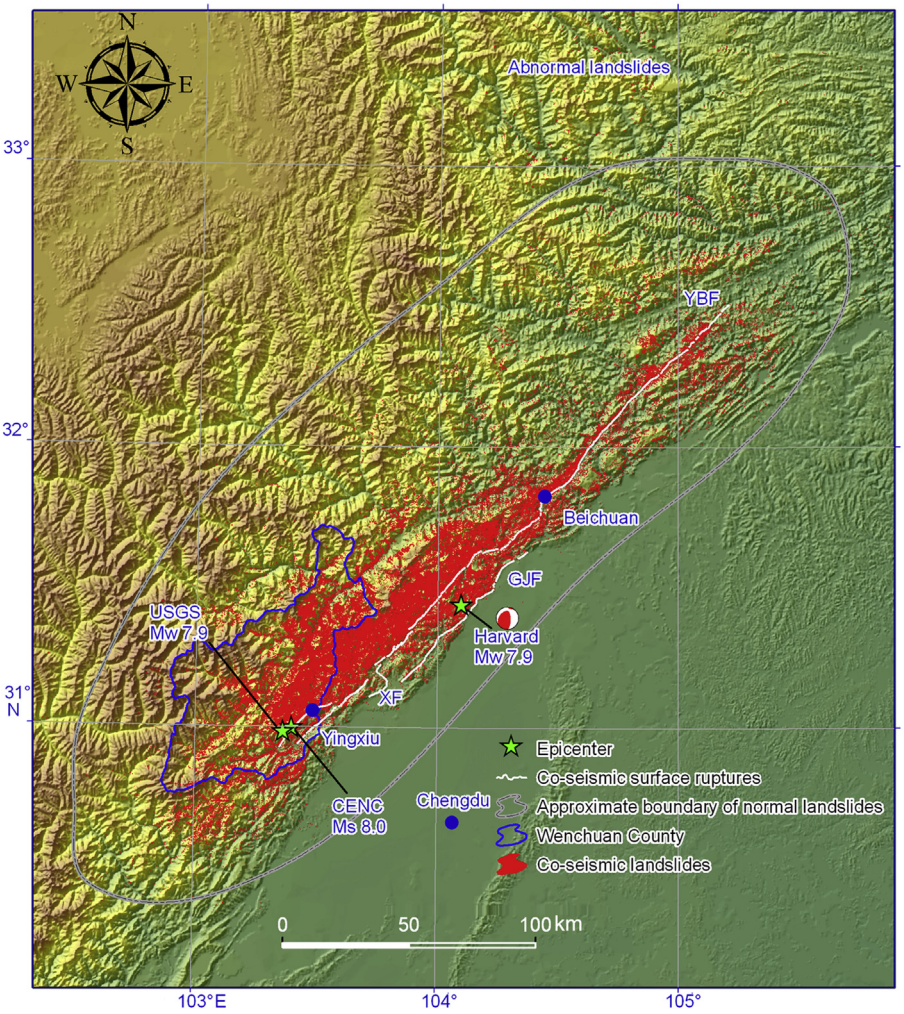

Figure 1. Spatial distribution of landslides triggered by the 2008 Wenchuan earthquake, China and remote images used for landslide visual interpretation pre- and post-earthquake. YBF is the Yingxiu-Beichuan fault; GJF is the Guanxian-Jiangyou fault; XF is the Xiaoyudong fault. USGS is U.S. Geological Survey; CENC is China Earthquake Network Center; Havard is Havard University.

the fault dominated by thrusting are much more than that on the northeastern section of the fault with dominant strike-slip.

4.2. The 2010 M_w 6.9 Yushu, China earthquake

The seismogenic fault of this event is the Ganzê-Yushu fault, which is the western section of the Xianshuihe fault zone of sinistral strike-slip (Chen et al., 2010; Sun et al., 2012). Based on visual interpretation of high-resolutions aerial photos and assisted by field investigations, a detailed landslide inventory related to the earthquake was constructed. It shows that the earthquake triggered at least 2036 landslides covering a total area of 1.194 km^2 (Fig. 2). These landslides were mainly distributed in a rectangle area of approximately 1500 km^2 (Xu et al., 2012d, 2013a). Images used for this earthquake event-based inventory map are aerial photographs in 0.2 m and 0.4 m resolutions, WorldView in 0.5 m resolution, and SPOT 5 in 2.5 m resolution (Xu et al., 2014b). Although boundaries of the landslides were delineated, they are presented in Fig. 2 by points rather than polygons because most of the landslides are of small sizes. Perhaps a few co-seismic landslides occurred out of the rectangle area, as available remote sensing images used to prepare the landslide inventory do not cover the regions out of the rectangle area aforementioned. Nevertheless, possible landslides out of the rectangle area should be few from the analysis using the law of landslide decay with distance to the seismogenic fault (Xu et al., 2013a).

4.3. The 2010 Haiti M_w 7.0 earthquake

This event occurred on a subduction zone between the North America plate and the Caribbean plate, in a complicated geologic context with multi-twisting compression. Initially, the Enriquillo-Plantain Garden fault (EPGF) was considered as the seismogenic fault (Fig. 3). Subsequent studies revealed that there is no surface rupture along this fault and the epicenter area. Finally, based on InSAR, GPS, and further filed investigations, it is thought that this event is attributed to a blind fault named the Léogâne fault sub-parallel to the EPGF (Calais et al., 2010; Hayes et al., 2010; Hough et al., 2010; Prentice et al., 2010). Visual interpretation of high-resolution remote sensing images on the Google Earth platform (last accessed September 2011) suggests 30,828 landslides triggered by the Haiti earthquake (Xu et al., 2012c). These landslides cover a total area of 15.736 km^2 and are distributed in an area about 3200 km^2 (Fig. 3).

4.4. The 2007 Chile M_w 6.2 earthquake

Focal mechanism of the 21 April 2007 event shows a rupture in a north-south direction, almost vertical plane, which coincides with the Liquiñe–Ofqui fault (Sepúlveda et al., 2010). Previous study (Sepúlveda et al., 2010) suggested that this earthquake triggered at least 500 landslides. A more detailed interpretation of landslides was conducted based on high-resolutions satellite images based on Google Earth platform (last accessed August 2012), and the resulting-inventory shows at least 1000 landslides triggered (Fig. 4). Most of these landslides occurred in a clustering manner.

5. Analysis and discussions

5.1. Comparison of the inventories

(1) The 2008 Wenchuan earthquake

After the May 12, 2008 earthquake occurred, some studies presented several point inventories of landslides triggered by this shock (e.g. Huang and Li, 2009a; Qi et al., 2010; Gorum et al., 2011). Their results showed that about 10,000 landslides based on emergency investigations, and about 60,000 landslides based on more

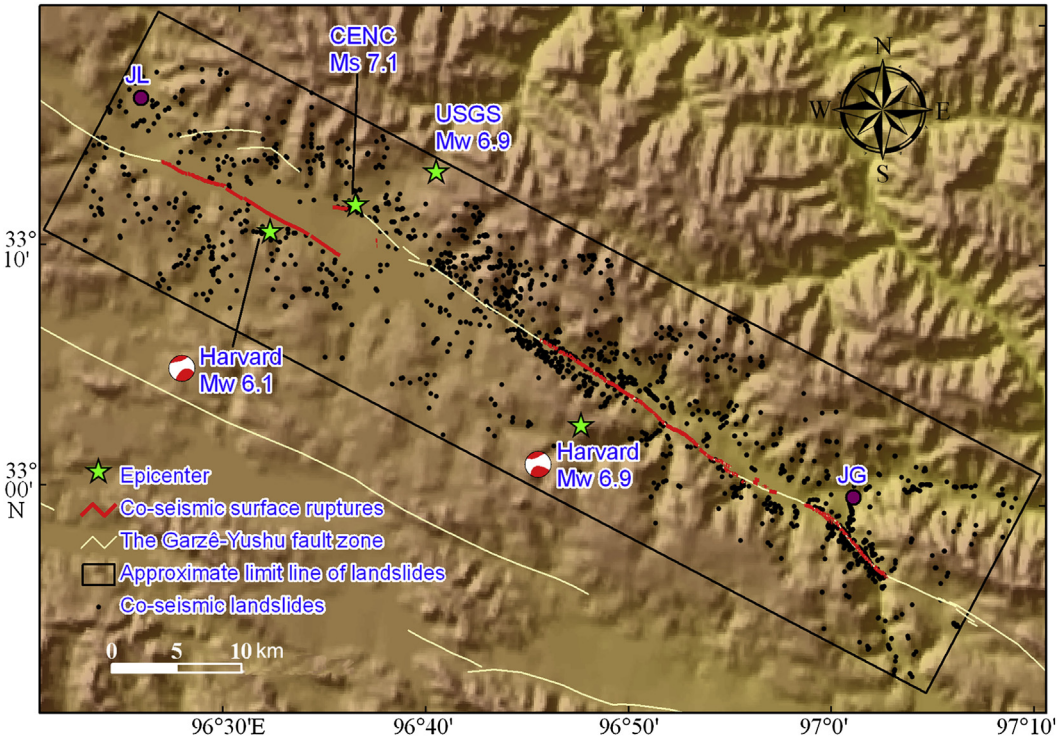

Figure 2. Spatial distribution of landslides triggered by the 2010 Yushu earthquake, China and coverage of remote sensing images post-earthquake. JL is the Jielong town and JG is the Jiegu town. USGS is U.S. Geological Survey; CENC is China Earthquake Network Center; Havard is Havard University.

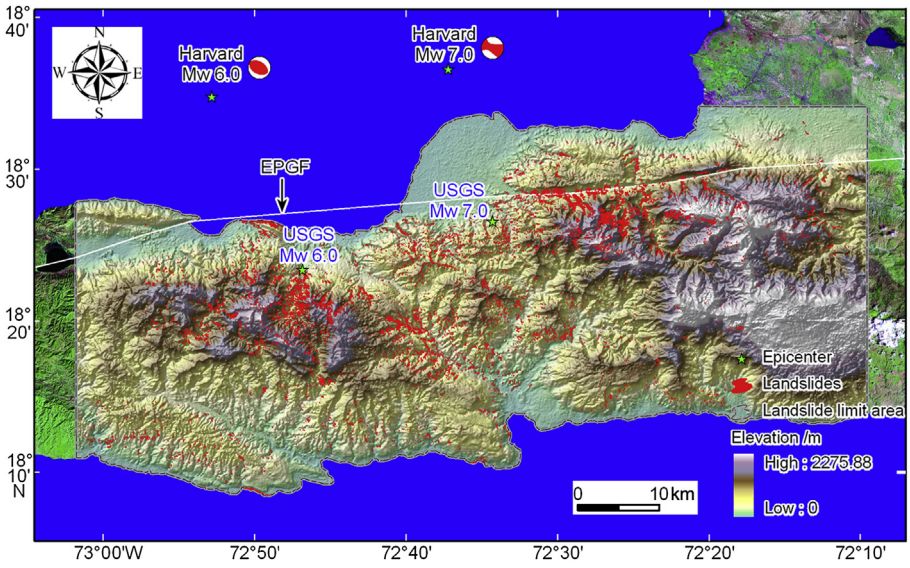

Figure 3. Spatial distribution of landslides triggered by the 2010 Haiti M_w 7.0 earthquake. Areas of blue color mean ocean. EPGF represents the Enriquillo-Plantain Garden fault. USGS is U.S. Geological Survey; Havard is Havard University.

careful and detailed interpretation of remote sensing images. Parker et al. (2011) obtained more than 60,000 landslide polygons using landslide satellite images and the automatic extraction method. In a preliminary effort, I delineated 50,000–60,000 landslides based on visual interpretation of remote sensing images with high resolution (Xu et al., 2009a, b; Dai et al., 2011). It seems that about 60,000 should be the real number of the Wenchuan earthquake-triggered landslides. However, there were some limitations in these results. For example, near the epicenter, some areas were not covered by my work due to lack of remote sensing images (Xu et al., 2009a, b; Dai et al., 2011), while these areas are the most serious affected by co-seismic landslides. On the other hand, some researchers delineate two or more individual landslides into one landslide. For instance, Parker et al. (2011) used the automatic extraction method to prepare the landslide inventory, in which several individual landslides were delineated into an individual landslide; one example is the Beichuan Middle School where the number of landslides was greatly reduced. For the point-based landslide inventory, such as Gorum et al. (2011), although it is difficult to quantitatively verify due to lake of source vector data, it can be inferred that some landslides were ignored in some landslide densely distribution areas. In other words, the number of landslides triggered by the Wenchuan earthquake should be much more than 60,000. This inference was verified by the latest studies (Xu and Xu, 2012a; Xu et al., 2014c) that demonstrate at least 197,481 landslides were caused by this huge shock.

(2) The 2010 Yushu, China M_w 6.9 earthquake

The investigation immediately after the event showed 282 landslides triggered by the earthquake (Yin et al., 2010). Subsequently, a detailed and careful visual interpretation of high-resolution aerial photos and satellite images suggested that at least 2036 landslides were triggered, verified by the field

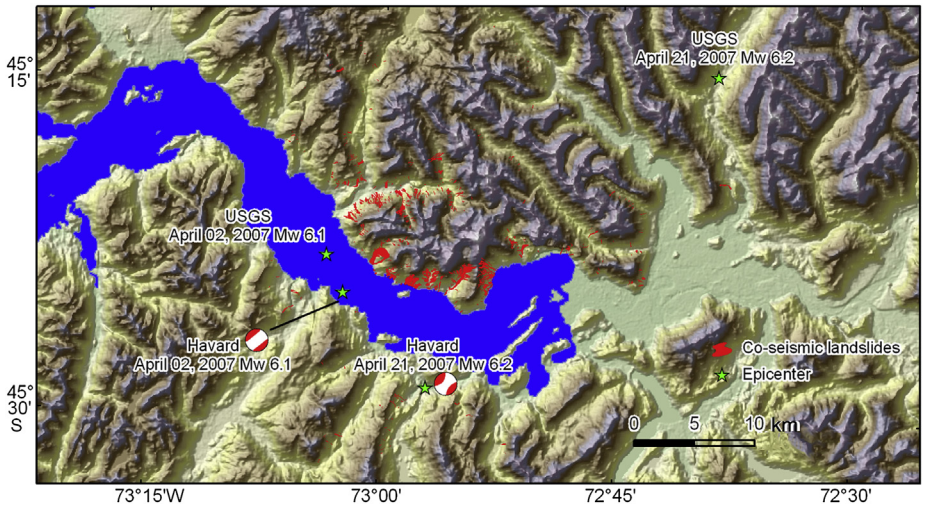

Figure 4. Inventory of landslides triggered by the 2007 Aysén Fjord earthquake, Chile. Areas of blue color mean water. USGS is U.S. Geological Survey; Harvard is Harvard University.

investigations (Xu et al., 2013a). Both results exhibit big differences, indicating that remote sensing and GIS technologies are essential tools for preparing a detailed and complete landslide inventory, which are quick and saving relative to field investigations. Especially, when a major earthquake occurs in an area of rugged mountains, difficult to access, like the 2010 Yushu, China event, the field survey must be replaced by space-based technologies.

(3) The 12 January 2010 Haiti M_w 7.0 earthquake

Harp et al. (2011b) suggested that at least 7000 landslides were triggered by this earthquake. Another inventory pointed out 4490 landslides were generated (Gorum et al., 2013). As stated previously, the author delineated 30,828 landslides triggered by this earthquake based on high-resolution images on the Google Earth platform. The possible reason for the differences may be that my work follows the following principles, while other researchers did not do so. (1) All landslides are delineated, including very small landslides. (2) The landslides on a same slope in my inventory are separated into individual landslides. (3) If a landslide exists on both pre-earthquake image and post-earthquake image, it is considered to occur before the earthquake if its shapes are the same in both images; otherwise the landslide is considered to be triggered by the earthquake. In addition, Harp et al. (2011b) used points to describe landslides, which might have led to missing of many small landslides

(4) The 21 April 2007 Chile M_w 6.2 earthquake

Sepúlveda et al. (2010) delineated 538 landslides triggered by the earthquake, whereas the author mapped at least 1000 landslides triggered by this event, considering all small-scale landslides.

5.2. The necessity to establish unified principles for preparing landslide inventories

Obvious differences in landslide inventories prepared by different researchers are due to inconsistent principles, including the methods and their criteria. It indicates the necessity to establish unified principles for landslide inventories. Harp et al. (2011a) have studied the landslide inventory criteria and mapping criteria. In a detailed review, Guzzetti et al. (2012) pointed out a lack of standards for preparation and update of landslide maps. In this paper, the author attempts to propose unified principles for preparing earthquake-landslide inventory maps. The author hopes that this issue will receive more attention and the commonly accepted principles would emerge in the future.

5.3. Significance of complete earthquake-landslide inventories

An inventory of earthquake-triggered landslides is the basis for seismic hazard assessment. Based on inventories, landslide susceptibility ranks can be determined through spatial distribution of landslides using GIS technology. Then, landslide susceptibility, hazard and risk analyses can be carried out. The scientific level of such studies is determined by the integrity and continuity of the landslide inventory. Some landslide spatial distribution and hazard assessment studies by using incomplete landslide inventories seem robust, because a large number of landslides are triggered and a large area is affected, leading to relatively little errors. However, some landslide inventories missing many landslides actually contain large errors. Therefore, it is important to prepare a detailed and completed landslide inventory for subsequent landslide spatial distribution analyses and hazard assessment.

Earthquake-triggered landslide inventories can help infer the earthquake magnitude, movement behavior of the causative fault, and seismic intensity. For example, Keefer (1984) established simple relationships between earthquake magnitude and landslide proxies, which include the distribution range, number, area, distance to the seismogenic fault, and the distance to earthquake source of landslides. Although these relationships are loose and not strict, earthquake magnitude can be probably inferred based on detailed earthquake-triggered landslide inventory maps. Some studies (e.g. Gorum et al., 2011, 2013; Xu and Xu, 2012a; Xu et al., 2014c) showed movement behavior of the seismogenic fault plays an important role in abundance of landslides triggered by earthquakes. There are obvious differences in landslide abundance and landslide distribution patterns related to earthquakes generated by thrusting, strike-slip, or blind faults, even if the earthquakes are of the similar magnitude. In addition, earthquake-triggered landslide spatial distribution data can reflect seismic intensity information (Xu et al., 2013b). Therefore, if information of an earthquake is not clear, e.g. ancient earthquakes, the earthquake-triggered landslide inventory can provide a reference to estimate its magnitude, seismogenic fault, and seismic intensity.

Detailed and objective earthquake-triggered landslide inventories are essential to the study of evolution of rivers and landscapes in the earthquake-struck area. Increasing studies show that a couple of opposite factors of crustal uplift and co-seismic landslides plays an important role in evolution of rivers and landscapes (Parker et al., 2011). Co-seismic landslide inventories are essential for volume calculation of co-seismic regional landslides. For example, Parker et al. (2011) discussed correlation of crustal uplift and total volume of landslides triggered by the 2008 Wenchuan earthquake in the Longmenshan mountain area. Their results showed the volume of regional landslides is larger than that of crustal uplift. However, their landslide inventory is obtained from automatic extraction of satellite images. Although their landslide inventory map is under manual inspection, there were obvious errors in it as several landslides were treated as an individual landslide, which resulted in an overestimated volume of regional landslides. Using a detailed inventory of landslides triggered by the 2008 Wenchuan earthquake, we estimated a volume of a landslide wasting mass only about 6 km^3 (Xu and Xu, 2013) much less than 9 km^3 by Parker et al. (2011), while the volume of co-seismic crustal uplift is merely 2.6 km^3. Further research on this issue would be significant to the prediction of the landscape evolution trend in the earthquake area.

5.4. Digitalization of historical paper-based landslide maps

For some historical earthquakes, most landslide inventory maps are paper-based due to limitation of computer technology of that time. Such paper-based inventory maps are valuable but can not directly be used for associated landslide spatial distribution analysis and hazard assessment. With the development and maturity of computer and GIS technologies, it is necessary to digitize such paper-based maps into computer-based digital maps. Fig. 5 is the digitized landslide inventory map of the May 1980 Mammoth Lakes, California, earthquake sequence, which was prepared from a paper-based landslide inventory map by Harp et al. (1984). The digital landslide inventory maps can enrich case studies of landslide inventories and can be used in subsequent scientific research.

6. Conclusions

The author presents detailed principles of preparing landslide inventory maps in this paper, including methods and criteria. Landslide identification should comply with the following principles: a map of all landslides is prepared as long as they can be

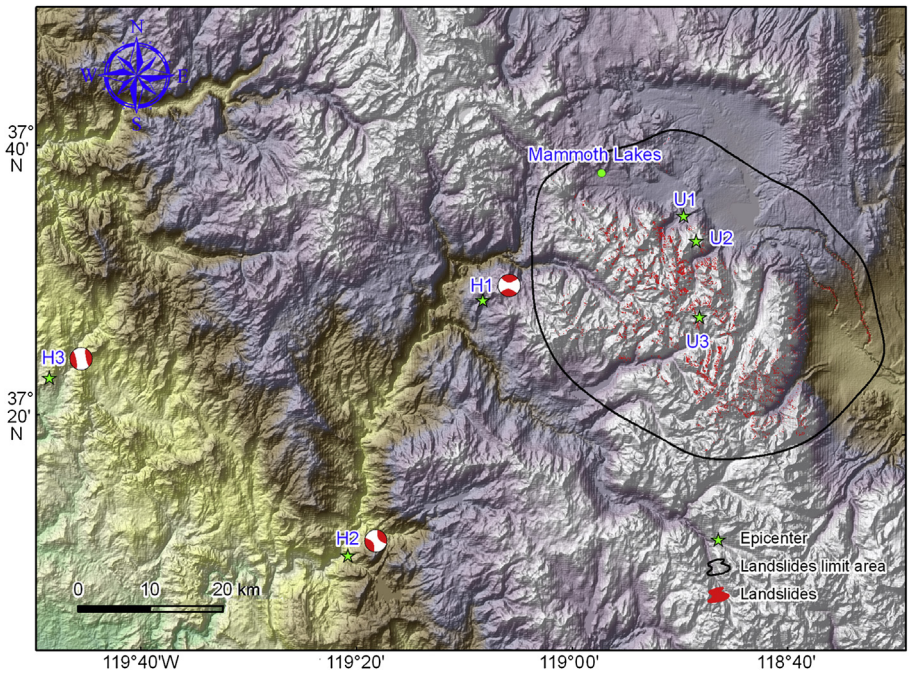

Figure 5. Landslides triggered by the May 1980 Mammoth Lakes, California, earthquake sequence. U1, U2, and U3 are the locations of the earthquake sequence from U.S. Geological Survey; H1, H2, and H3 are the locations of the earthquake sequence from Harvard University.

recognized from images; both the landslide boundary and position of the landslide source area should be mapped; spatial distribution of landslides should be continuous; complex landslides should be separated into individual landslides; three types of errors, i.e. precision of location and boundary of landslides, false positive errors, and false negative errors, which influence earthquake-triggered landslides inventories, should be considered; and inventories of co-seismic landslides should be constructed by the visual interpretation method rather than automatic identification. In addition, some issues of selecting remote sensing images and building landslides attribute database are also addressed in this paper.

With the proposed principles, the author presents four earthquake-triggered landslides inventories related to four recent major earthquakes. The results show that at least 197,481 landslides were triggered by the May 12, 2008 Wenchuan, China M_w 7.9, at least 2036 triggered by the April 14, 2010 Yushu, China M_w 6.9, 30,828 landslides triggered by the January 12, 2010 Haiti M_w 7.0, and about 1000 landslides triggered by the Aysén Fjord, Chile M_w 6.2, respectively. These landslide inventories have great significance for the research of landslide spatial distribution and hazard assessment, prevention and mitigation of landslides and debris flow disaster in earthquake struck areas. These data can help infer earthquake magnitude, movement behavior of the active fault, and seismic intensity. They are also essential to the study of evolution of rivers and landscapes in the earthquake struck area.

Because of lack of unified principles for preparing earthquake-triggered landslide inventories, the previous results of different authors on the same events contain obvious differences. One of the purposes of this paper is to emphasize the necessity to establish unified principles for preparing earthquake-triggered landslide inventories, which would make the future landslide inventor maps more objective and consistent.

Acknowledgments

This research was supported by the National Natural Science Foundation of China (Grant No. 41202235).

References

Adams, J., 1980. Contemporary uplift and erosion of the Southern Alps, New Zealand: summary. Geological Society of America Bulletin 91 (1), 2–4.

Alfaro, P., Delgado, J., García-Tortosa, F.J., Lenti, L., López, J.A., López-Casado, C., Martino, S., 2012. Widespread landslides induced by the M_w 5.1 earthquake of 11 May 2011 in Lorca, SE Spain. Engineering Geology 137–138, 40–52.

Calais, E., Freed, A., Mattioli, G., Amelung, F., Jónsson, S., Jansma, P., Hong, S.H., Dixon, T., Prépetit, C., Momplaisir, R., 2010. Transpressional rupture of an unmapped fault during the 2010 Haiti earthquake. Nature Geoscience 3 (11), 794–799.

Chen, L.C., Wang, H., Ran, Y.K., Sun, X.Z., Su, G.W., Wang, J., Tan, X.B., Li, Z.M., Zhang, X.Q., 2010. The M_s 7.1 Yushu earthquake surface rupture and large historical earthquakes on the Garzê-Yushu Fault. Chinese Science Bulletin 55 (31), 3504–3509.

Chigira, M., Yagi, H., 2006. Geological and geomorphological characteristics of landslides triggered by the 2004 Mid Niigta prefecture Earthquake in Japan. Engineering Geology 82 (4), 202–221.

Dai, F.C., Xu, C., Yao, X., Xu, L., Tu, X.B., Gong, Q.M., 2011. Spatial distribution of landslides triggered by the 2008 M_s 8.0 Wenchuan earthquake, China. Journal of Asian Earth Sciences 40 (4), 883–895.

Fukuoka, H., Sassa, K., Scarascia-Mugnozza, G., 1997. Distribution of landslides triggered by the 1995 Hyogo-ken Nanbu Earthquake and long runout mechanism of the Takarazuka Golf Course landslide. Journal of Physics of the Earth 45 (2), 83–90.

Gorum, T., Fan, X.M., van Westen, C.J., Huang, R.Q., Xu, Q., Tang, C., Wang, G.H., 2011. Distribution pattern of earthquake-induced landslides triggered by the 12 May 2008 Wenchuan earthquake. Geomorphology 133 (3), 152–167.

Gorum, T., van Westen, C.J., Korup, O., van der Meijde, M., Fan, X.M., van der Meer, F.D., 2013. Complex rupture mechanism and topography control symmetry of mass-wasting pattern, 2010 Haiti earthquake. Geomorphology 184, 127–138.

Govi, M., 1977. Photo-interpretation and mapping of the landslides triggered by the Friuli earthquake (1976). Bulletin of the International Association of Engineering Geology 15 (1), 67–72.

Guzzetti, F., Mondini, A.C., Cardinali, M., Fiorucci, F., Santangelo, M., Chang, K.T., 2012. Landslide inventory maps: new tools for an old problem. Earth-Science Reviews 112 (1–2), 42–66.

Harp, E.L., Wieczorek, G.F., Wilson, R.C., 1978. Earthquake-induced Landslides from the February 4, 1976 Guatemala Earthquake and Their Implications for Landslide Hazard Reduction. US Geological Survey, Washington. Document number: 5175.

Harp, E.L., Wilson, R.C., Wieczorek, G.F., 1981. Landslides from the February 4, 1976, Guatemala Earthquake. US Geological Survey, Washington.

Harp, E.L., Tanaka, K., Sarmiento, J., Keefer, D.K., 1984. Landslides from the May 25–27, 1980, Mammoth Lakes, California, Earthquake Sequence. US Geological Survey. Miscellaneous Investigations Series Map I-1612, Reston Va: The Survey; Denver, CO: For Sale by Branch of Distribution, Scale 1: 62, 500.

Harp, E.L., Keefer, D.K., 1989. Earthquake-induced Landslides, Mammoth Lakes Area, California in Landslides in Central California: San Francisco and Central California//Brown III W M. Field Trip Guideb, vol. T381, AGU, Washington D C, 48–53. http://dx.doi.org/10.1029/FT381p0048.
Harp, E.L., Jibson, R.W., 1995. Inventory of landslides triggered by the 1994 Northridge, California Earthquake. USGS. http://geo-nsdi.er.usgs.gov/metadata/open-file/95-213/.
Harp, E.L., Jibson, R.W., 1996. Landslides triggered by the 1994 Northridge, California, Earthquake. Bulletin of the Seismological Society of America 86 (1B), S319–S332.
Harp, E.L., Keefer, D.K., Sato, H.P., Yagi, H., 2011a. Landslide inventories: the essential part of seismic landslide hazard analyses. Engineering Geology 122 (1), 9–21.
Harp, E.L., Jibson, R.W., Dart, R.L., 2011b. The Effect of Complex Fault Rupture on the Distribution of Landslides Triggered by the 12 January 2010, Haiti Earthquake. Proceedings of the Second World Landslide Forum, Rome: October 3–7, 2011.
Hayes, G.P., Briggs, R.W., Sladen, A., Fielding, E.J., Prentice, C., Hudnut, K., Mann, P., Taylor, F.W., Crone, A.J., Gold, R., Ito, T., Simons, M., 2010. Complex rupture during the 12 January 2010 Haiti earthquake. Nature Geoscience 3 (11), 800–805.
Hough, S.E., Altidor, J.R., Anglade, D., Given, D., Janvier, M.G., Maharrey, J.Z., Meremonte, M., Mildor, B.S.L., Prepetit, C., Yong, A., 2010. Localized damage caused by topographic amplification during the 2010 *M* 7.0 Haiti earthquake. Nature Geoscience 3 (11), 778–782.
Huang, R.Q., Li, W.L., 2009a. Analysis on the number and density of landslides triggered by the 2008 Wenchuan earthquake, china. Journal of Geological Hazards and Environment Preservation 20 (3), 1–7 (in Chinese).
Huang, R.Q., Li, W.L., 2009b. Analysis of the geo-hazards triggered by the 12 May 2008 Wenchuan earthquake, China. Bulletin of Engineering Geology and the Environment 68 (3), 363–371.
Jibson, R.W., Keefer, D.K., 1989. Statistical analysis of factors affecting landslide distribution in the new Madrid seismic zone, Tennessee and Kentucky. Engineering Geology 27 (1–4), 509–542.
Jibson, R.W., Harp, E.L., 1994. Landslides triggered by the Northridge Earthquake. Earthquake & Volcanoes 25 (1), 31–41.
Jibson, R.W., Harp, E.L., 2012. Extraordinary distance limits of landslides triggered by the 2011 Mineral, Virginia, Earthquake. Bulletin of the Seismological Society of America 102 (6), 2368–2377.
Kamp, U., Growley, B.J., Khattak, G.A., Owen, L.A., 2008. GIS-based landslide susceptibility mapping for the 2005 Kashmir earthquake region. Geomorphology 101 (4), 631–642.
Keefer, D.K., 1984. Landslides caused by earthquakes. Geological Society of America Bulletin 95 (4), 406–421.
Keefer, D.K., 1999. Earthquake-induced landslides and their effects on alluvial fans. Journal of Sedimentary Research 69 (1), 84–104.
Keefer, D.K., 2000. Statistical analysis of an earthquake-induced landslide distribution—the 1989 Loma Prieta, California event. Engineering Geology 58 (3–4), 231–249.
Keefer, D.K., 2002. Investigating landslides caused by earthquakes – a historical review. Surveys in Geophysics 23 (6), 473–510.
Khazai, B., Sitar, N., 2004. Evaluation of factors controlling earthquake-induced landslides caused by Chi-Chi Earthquake and comparison with the Northridge and Loma Prieta events. Engineering Geology 71 (1–2), 79–95.
Liao, H.W., Lee, C.T., 2000. Landslides Triggered by the Chi-Chi Earthquake [EB/OL]. ACRS. http://www.geospatialworld.net.
Mahesh, P., Kundu, B., Catherine, J.K., Gahalaut, V.K., 2011. Anatomy of the 2009 Fiordland earthquake (M_w 7.8), South Island, New Zealand. Geoscience Frontiers 2 (1), 17–22.
Martha, T.R., Kerle, N., van Westen, C.J., Jetten, V., Kumar, K.V., 2012. Object-oriented analysis of multi-temporal panchromatic images for creation of historical landslide inventories. ISPRS journal of photogrammetry and remote sensing 67, 105–119.
Martha, T.R., Govindharaj, K.B., Kumar, K.V., 2015. Damage and geological assessment of the 18 September 2011 Mw 6.9 earthquake in Sikkim, India using very high resolution satellite data. Geoscience Frontiers 6, 793–806. http://dx.doi.org/10.1016/j.gsf.2013.12.011.
Marzorati, S., Luzi, L., Amicis, M.D., 2002. Rock falls induced by earthquakes: a statistical approach. Soil Dynamics and Earthquake Engineering 22 (7), 565–577.
Moosavi, V., Talebi, A., Shirmohammadi, B., 2014. Producing a landslide inventory map using pixel-based and object-oriented approaches optimized by Taguchi method. Geomorphology 204, 646–656.
Morimoto, R., 1951. Geology of Imaichi district with special reference to the earthquake of Dec. 26, 1949 (II). Departmental Bulletin Paper 29 (2), 349–358.
Morton, D.M., 1971. Seismically triggered landslides above San Fernando Valley. California Geology 24 (4–5). Special San Fernando Earthquake Edition.
Owen, L.A., Kamp, U., Khattak, G.A., Harp, E.L., Keefer, D.K., Bauer, M.A., 2008. Landslides triggered by the 8 October 2005 Kashmir earthquake. Geomorphology 94 (1–2), 1–9.
Parise, M., Jibson, R.W., 2000. A seismic landslide susceptibility rating of geologic units based on analysis of characteristics of landslides triggered by the 17 January, 1994 Northridge, California earthquake. Engineering Geology 58 (3–4), 251–270.
Parker, R.N., Densmore, A.L., Rosser, N.J., de Michele, M., Li, Y., Huang, R.Q., Whadcoat, S., Petley, D.N., 2011. Mass wasting triggered by the 2008 Wenchuan earthquake is greater than orogenic growth. Nature Geoscience 4 (7), 449–452.
Pearce, A.J., O'Loughlin, C.L., 1985. Landsliding during a *M* 7.7 Earthquake: influence of geology and topography. Geology 13 (12), 855–858.
Pearce, A.J., Watson, A.J., 1986. Effects of earthquake-induced landslides on sediment budget and transport over a 50-yr period. Geology 14 (1), 52–55.
Plafker, G., Ericksen, G.E., Fernández Concha, J., 1971. Geological aspects of the May 31, 1970, Peru earthquake. Bulletin of the Seismological Society of America 61 (3), 543–578.
Prentice, C., Mann, P., Crone, A., Gold, R.D., Hudnut, K.W., Briggs, R.W., Koehler, R.D., Jean, P., 2010. Seismic hazard of the Enriquillo-Plantain Garden fault in Haiti inferred from palaeoseismology. Nature Geoscience 3 (11), 789–793.
Pourghasemi, H.R., Mohammady, M., Pradhan, B., 2012. Landslide susceptibility mapping using index of entropy and conditional probability models in GIS: Safarood Basin, Iran. Catena 97, 71–84.
Pradhan, B., Lee, S., 2007. Utilization of optical remote sensing data and GIS tools for regional landslide hazard analysis using an artificial neural network model. Earth Science Frontiers 14 (6), 143–151.
Pradhan, B., Lee, S., 2010. Landslide susceptibility assessment and factor effect analysis: backpropagation artificial neural networks and their comparison with frequency ratio and bivariate logistic regression modelling. Environmental Modelling & Software 25 (6), 747–759.
Qi, S.W., Xu, Q., Lan, H.X., Zhang, B., Liu, J.Y., 2010. Spatial distribution analysis of landslides triggered by 2008.5.12 Wenchuan earthquake, China. Engineering Geology 116 (1), 95–108.
Rodriguez, C.E., Bommer, J.J., Chandler, R.J., 1999. Earthquake-induced landslides: 1980–1997. Soil Dynamics and Earthquake Engineering 18 (5), 325–346.
Sassa, K., 2005. Landslide disasters triggered by the 2004 Mid-Niigata Prefecture earthquake in Japan. Landslides 2 (2), 135–142.
Sato, H.P., Sekiguchi, T., Kojiroi, R., Suzuki, Y., Iida, M., 2005. Overlaying landslides distribution on the earthquake source, geological and topographical data: the Mid Niigata prefecture earthquake in 2004, Japan. Landslides 2 (2), 143–152.
Sato, H.P., Hasegawa, H., Fujiwara, S., Tobita, M., Koarai, M., Une, H., Iwahashi, J., 2007. Interpretation of landslide distribution triggered by the 2005 Northern Pakistan earthquake using SPOT 5 imagery. Landslides 4 (2), 113–122.
Schuster, R.L., Nieto, A.S., O'Rourke, T.D., Crespo, E., Plaza-Nieto, G., 1996. Mass wasting triggered by the 5 March 1987 Ecuador earthquakes. Engineering Geology 42 (1), 1–23.
Sekiguchi, T., Sato, H.P., 2006. Feature and distribution of landslides induced by the Mid Niigata Prefecture Earthquake in 2004, Japan. Journal of the Japan Landslide Society 43 (3), 142–154.
Sepúlveda, S.A., Serey, A., Lara, M., Pavez, A., Rebolledo, S., 2010. Landslides induced by the April 2007 Aysén Fjord earthquake, Chilean Patagonia. Landslides 7 (4), 483–492.
Sun, X.Z., Xu, X.W., Chen, L.C., Tan, X.B., Yu, G.H., Li, Z.M., Su, G.W., Wang, J., Zhang, X.Q., 2012. Surface rupture features of the 2010 Yushu earthquake and its tectonic implication. Chinese Journal of Geophysics 55 (1), 155–170 (in Chinese).
Tan, X.B., Yuan, R.M., Xu, X.W., Chen, G.H., Klinger, Y., Chang, C.P., Ren, J.J., Xu, C., Li, K., 2012. Complex surface rupturing and related formation mechanisms in the Xiaoyudong area for the 2008 Mw 7.9 Wenchuan Earthquake, China. Journal of Asian Earth Sciences 58, 132–142.
Tibaldi, A., Ferrari, L., Pasquare, G., 1995. Landslides triggered by earthquakes and their relations with faults and mountain slope geometry: an example from Ecuador. Geomorphology 11 (3), 215–226.
Varnes, D.J., 1978. Slope Movement Types and Processes. Transportation Research Board Special Report. trid.trb.org.
Wang, W.N., Nakamura, H., Tsuchiya, S., Chen, C.C., 2002. Distributions of landslides triggered by the Chi-chi Earthquake in Central Taiwan on September 21, 1999. Landslides-Journal of the Japan Landslide Society 38 (4), 18–26.
Wang, W.N., Wu, H.L., Nakamura, H., Wu, S.C., Ouyang, S., Yu, M.F., 2003. Mass movements caused by recent tectonic activity: the 1999 Chi-Chi Earthquake in central Taiwan. The Island Arc 12 (4), 325–334.
Wang, H.B., Sassa, K., Xu, W.Y., 2007. Analysis of a spatial distribution of landslides triggered by the 2004 Chuetsu earthquakes of Niigata Prefecture, Japan. Natural Hazards 41 (1), 43–60.
Wasowski, J., Gaudio, V.D., Pierri, P., Capolongo, D., 2002. Factors controlling seismic susceptibility of the Sele Valley slopes: the case of the 1980 Irpinia earthquake re-examined. Surveys in Geophysics 23 (6), 563–593.
Xu, C., 2013a. Earthquake-triggered Landslide Susceptibility Mapping in the 2010 Yushu, China Earthquake Struck Area Using Artificial Neural Network Model. Global View of Engineering Geology and the Environment. Taylor & Francis Group, London, ISBN 978-1-138-00078-0, pp. 217–223.
Xu, C., 2013b. Assessment of earthquake-triggered landslide susceptibility based on expert knowledge and information value methods: a case study of the 20 April 2013 Lushan, China M_w 6.6 earthquake. Disaster Advances 6 (13), 119–130.
Xu, C., 2013c. Correlations of Earthquake-triggered Landslides Volume and Seismogenic Fault: a Case Study of the 12 May 2008 Wenchuan Earthquake, China. Global View of Engineering Geology and the Environment. Taylor & Francis Group, London, ISBN 978-1-138-00078-0, pp. 93–98.
Xu, C., Xu, X.W., 2012a. Comment on "Spatial distribution analysis of landslides triggered by 2008.5. 12 Wenchuan earthquake, China" by Shengwen Qi, Qiang Xu, Hengxing Lan, Bing Zhang, Jianyou Liu. Engineering Geology 116 (2010), 95–108. Engineering Geology 133, 40–42.
Xu, C., Xu, X.W., 2012b. Spatial distribution of seismic landslides and their erosion thickness relate with a transpressional fault caused earthquake of subduction zone. Journal of Engineering Geology 20 (5), 732–744 (in Chinese).

Xu, C., Xu, X.W., 2013. Response rate of seismic slope mass movements related with the 2008 Wenchuan earthquake and its spatial distribution analysis. Chinese Journal of Rock Mechanics and Engineering 32 (S2), 3888–3908 (in Chinese).

Xu, C., Xu, X., 2014a. The spatial distribution pattern of landslides triggered by the 20 April 2013 Lushan earthquake of China and its implication to identification of the seismogenic fault. Chinese Science Bulletin 59 (13), 1416–1424. http://dx.doi.org/10.1007/s11434-014-0202-0.

Xu, C., Xu, X.W., 2014b. Statistical analysis of landslides caused by the M_w 6.9 Yushu, China, earthquake of April 14, 2010. Natural Hazards. http://dx.doi.org/10.1007/s11069-014-1038-2.

Xu, C., Dai, F.C., Yao, X., 2009a. Incidence number and affected area of Wenchuan earthquake-induced landslides. Science & Technology Review 27 (11), 79–81 (in Chinese).

Xu, C., Dai, F.C., Chen, J., Tu, X.B., Xu, L., Li, W.C., Tian, W., Cao, Y.B., Yao, X., 2009b. Identification and analysis of secondary geological hazards triggered by a magnitude 8.0 Wenchuan earthquake. Journal of Remote Sensing 13 (4), 754–762 (in Chinese).

Xu, X.W., Wen, X.Z., Yu, G.H., Chen, G.H., Klinger, Y., Hubbard, J., Shaw, J., 2009c. Coseismic reverse- and oblique-slip surface faulting generated by the 2008 M_w 7.9 Wenchuan earthquake, China. Geology 37 (6), 515–518.

Xu, C., Dai, F.C., Xu, X.W., 2010. Wenchuan earthquake induced landslides: an overview. Geological Review 56 (6), 860–874 (in Chinese).

Xu, C., Dai, F.C., Xu, X.W., Lee, Y.H., 2012a. GIS-based support vector machine modeling of earthquake-triggered landslide susceptibility in the Jianjiang River watershed, China. Geomorphology 145–146, 70–80.

Xu, C., Xu, X.W., Dai, F.C., Saraf, A.K., 2012b. Comparison of different models for susceptibility mapping of earthquake triggered landslides related with the 2008 Wenchuan earthquake in China. Computers & Geosciences 46, 317–329.

Xu, C., Xu, X.W., Yu, G.H., 2012c. Earthquake triggered landslide hazard mapping and validation related with the 2010 Port-au-Prince, Haiti earthquake. Disaster Advances 5 (4), 1297–1304.

Xu, C., Xu, X.W., Lee, Y.H., Tan, X.B., Yu, G.H., Dai, F.C., 2012d. The 2010 Yushu earthquake triggered landslide hazard mapping using GIS and weight of evidence modeling. Environmental Earth Sciences 66 (6), 1603–1616.

Xu, C., Xu, X.W., Yu, G.H., 2013a. Landslides triggered by slipping-fault-generated earthquake on a plateau: an example of the 14 April 2010, M_s 7.1, Yushu, China earthquake. Landslides 10 (4), 421–431.

Xu, C., Xu, X.W., Zhou, B.G., Yu, G.H., 2013b. Revisions of the M 8.0 Wenchuan earthquake seismic intensity map based on co-seismic landslide abundance. Natural Hazards 69 (3), 1459–1476.

Xu, C., Shyu, J.B.H., Xu, X.W., 2014a. Landslides triggered by the 12 January 2010 M_w 7.0 Port-au-Prince, Haiti, earthquake: visual interpretation, inventory compiling and spatial distribution statistical analysis. Natural Hazards and Earth System Sciences & Discussions 2 (2), 1259–1331.

Xu, C., Xu, X.W., Pourghasemi, H.R., Pradhan, B., Iqbal, J., 2014b. Volume, gravitational potential energy reduction, and regional centroid position change in the wake of landslides triggered by the 14 April 2010 Yushu earthquake of China. Arabian Journal of Geosciences 7 (6), 2129–2138. http://dx.doi.org/10.1007/s12517-013-1020-4.

Xu, C., Xu, X.W., Yao, X., Dai, F.C., 2014c. Three (nearly) complete inventories of landslides triggered by the May 12, 2008 Wenchuan M_w 7.9 earthquake of China and their spatial distribution statistical analysis. Landslides 11 (3), 441–461. http://dx.doi.org/10.1007/s10346-013-0404-6.

Yagi, H., Higaki, D., Yamamoto, M., Yamasaki, T., 2009. Distribution and characteristics of landslides induced by the Iwate–Miyagi Nairiku Earthquake in 2008 in Tohoku District, Northeast Japan. Landslides 6 (4), 335–344.

Yin, Y.P., Zhang, Y.S., Ma, Y.S., Hu, D.G., Zhang, Z.C., 2010. Research on major characteristics of geohazards induced by the Yushu M_s 7.1 earthquake. Journal of Engineering Geology 18 (3), 289–296 (in Chinese).